Dean Vortex Stability Using Magnetic Resonance Flow Imaging and Numerical Analysis

Hanuman Mallubhotla and Georges Belfort
Howard P. Isermann Dept. of Chemical Engineering, Rensselaer Polytechnic Institute, Troy, NY 12180

William A. Edelstein and Thomas A. Early
GE Corporate Research & Development, Schenectady, NY 12301

Magnetic resonance flow imaging using flow encoding with spin warp imaging was used in three dimensions to measure velocity profiles and the dynamic behavior of centrifugally-induced (Dean) vortices in curved tube flow. Experimental measurements were compared with numerical simulations obtained from the solution of Navier-Stokes and continuity equations using a commercial finite-element package. Effects of flow rate and geometry, and the ratio of the tube radius to that of curvature on the stability of Dean vortices were studied. Twisting and bifurcation of vortices increased with increasing flow rate and radius ratio. A six-vortex pattern was measured experimentally and predicted numerically. Additional wall shear rates, due to Dean vortices, were estimated from velocity measurements in the cross-sectional plane. A phase diagram was constructed to establish conditions for the existence of two, four or six vortices as a function of flow rate and curvature. Experimental observations were compared with numerical results obtained from three types of finite-element grids. The full-tube grid without symmetry planes was most predictive for vortex bifurcation, while the pseudo-cylindrical full-tube grid with a plane of symmetry gave best results for shear rates. Results from the numerical analysis agreed qualitatively well with the MRI measurements.

Introduction

Various approaches have been used to reduce concentration polarization and fouling in membrane processes. These include chemical modification of the membrane surface, physical methods such as scouring with sponge balls, and hydrodynamic methods such as the use of eddies during turbulent flow (Belfort, 1989).

One of the most successful depolarizing methods has been the use of well-ordered Taylor vortices established in a rotating annular filter module. The rotating filter has been applied successfully to enzyme fractionation, cell harvesting cell debris removal, and even diagnosis of fouling (Kroner and Nissinen, 1985; Kroner et al., 1987; Belfort et al., 1993a,b). However, any design based on rotating a membrane module will require substantially more energy than stationary systems. Furthermore, the complexity and sealing difficulties with rotating module systems has limited large-scale commercial development.

An alternate method of establishing centrifugal vortices resulting from unstable flow in spiral wound membrane ducts has been investigated by Belfort and co-workers (Brewster et al., 1993; Chung, 1992; Chung et al., 1993a,b,c, 1996, 1998; Gehlert et al., 1998; Kluge et al., 1999a,b; Luque et al., 1999; Mallubhotla et al., 1995, 1998, 1999; Mallubhotla and Belfort, 1997; Belfort et al., 1993c; Belfort, 1997). Such Dean vortex flow has similar advantages to Taylor vortex flow, but is also amenable to scale-up (Moulin et al., 1999). In addition, it is

Correspondence concerning this article should be addressed to G. Belfort.
Current address of H. Mallubhotla: Prodigene, Inc., College Station, TX 77845.

not expected to consume unreasonable amounts of energy or have sealing difficulties (Bubolz et al., 1998).

Although optical methods have been successfully used to measure vortex behavior in curved channel flow (Chung, 1992; Cheng and Mok, 1984), these methods are limited due to the low accuracy of measurement. While hot-wire methods are accurate, they are invasive (Kelleher et al., 1980). Laser Doppler Velocimetry has been extensively used for determining flow fields and time-dependent flows. It is, however, limited by the need for transparent containers and solutions. With our long-term interest in fluid flow of particulate suspensions in membrane modules containing opaque hollow fiber or spiral wound flat sheet membranes, magnetic resonance flow imaging (MRFI) provides a noninvasive and facile method to obtain three-dimensional flow fields without the limitations of transparency. Our group has pioneered the use of MRFI for studying flows in hollow fiber membrane modules (Heath et al., 1990; Hammer et al., 1990). This technique can thus be used effectively to study the 3-D behavior of flow in curved tubes.

Bottomley (1982) gives an excellent review of the history of nuclear magnetic resonance (NMR) imaging techniques. He also provides an outline of imaging instrumentation. Battocletti (1984) gives a listing of MRI installations and discusses the evolution of proton imaging. MRFI was used to study the behavior of Taylor vortex systems (Vera-Colon, 1986). Caprihan and Fukushima (1990) review the methods of flow measurement by NMR. Heath et al. (1990) and Hammer et al. (1990) measured the fluid velocity profile in the extracapillary space of a hollow fiber bioreactor. Pangrle et al. (1992) investigated the steady, laminar, incompressible fluid flow in a porous tube and shell system by using a time of flight (TOF) technique. NMR flow micro-imaging has been used to measure the thickness of oil concentration polarization layers in hollow fiber membranes (Yao, 1995).

Chung et al. (1993c) have studied the velocity profiles for flow in a curved slit by MRFI. By measuring the mean velocity profiles in a curved slit, they have verified the existence and the onset of Dean vortices. They have also determined the rate of decay and the length of persistence of Dean vortices in a straight channel placed after a 180° curved slit. Using 2-D and 3-D NMR pulse sequences, Chung et al. (1993b) have measured the velocity profiles for flow in a curved U-tube. The 2-D pulse sequence was sufficient to measure the axial velocity profiles accurately, while a 3-D pulse sequence was necessary to obtain the transverse velocities. This was because the transverse velocities induced by Dean vortices were an order of magnitude smaller than the axial velocities.

The work reported here follows our earlier effort and has the goal of analyzing flow in a curved tube with centrifugal instabilities (Dean vortices) through experimental observation using MRFI and numerical simulation. In this study, the work of Chung et al. (1993b) was extended. Both axial and transverse velocity profiles were measured for five tubes of different radius ratios, as a function of increasing flow rate. Wall shear rates were also measured.

The magnetic resonance imaging and numerical methods employed in this study have been discussed in detail by Chung et al. (1993b).

Numerical Studies

Numerical studies were undertaken to simulate the behavior of flow in curved tubes. Details of the numerical methods were given by Chung et al. (1993b). The main differences between the numerical analysis reported here and that of our previous study were the use of a different inlet condition and the use of several grids. Instead of using a parabolic velocity profile at the entrance, as was assumed by Chung et al. (1993b), a constant inlet velocity was specified here. Usual assumptions of Newtonian flow, no-slip at wall, and so on, were the same. The inlet section of the finite-element grid was made sufficiently long such that a nearly parabolic profile was developed at the entrance to the curved section. Also,

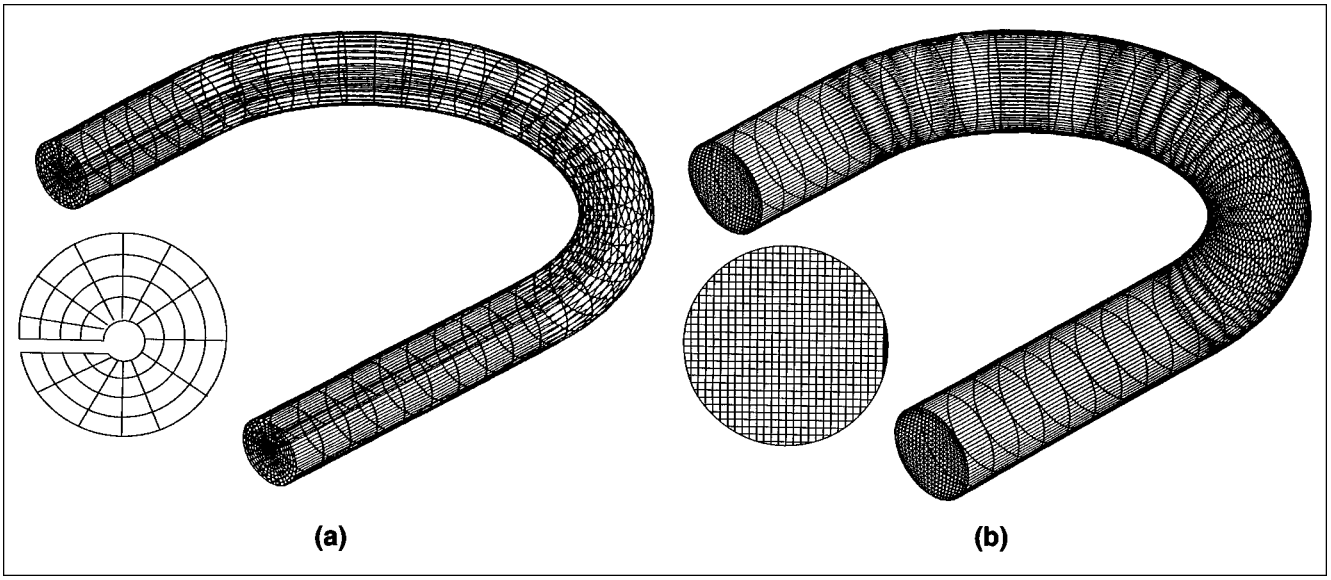

Figure 1. Finite-element grid for the numerical analysis:
(a) Full grid with a plane of symmetry; (b) full-grid without a plane of symmetry.

Table 1. Dimensions of Glass U-Tubes

Tube Radius a (mm)	Radius of Curvature, r_c (mm)	Radius Ratio, (a/r_c)
4.15	49.5	0.084
3.90	25.40	0.154
9.32	48.52	0.192
4.18	16.25	0.258
8.02	25.30	0.317

the curved sections in both numerical and experimental work were sufficiently long to allow full flow development. Lengths of these sections were roughly an order of magnitude larger than the diameter of curvature (Keulegan and Beij, 1937). Whenever symmetry planes are used in the formulation of the finite-element grid, the symmetry boundary condition was applied.

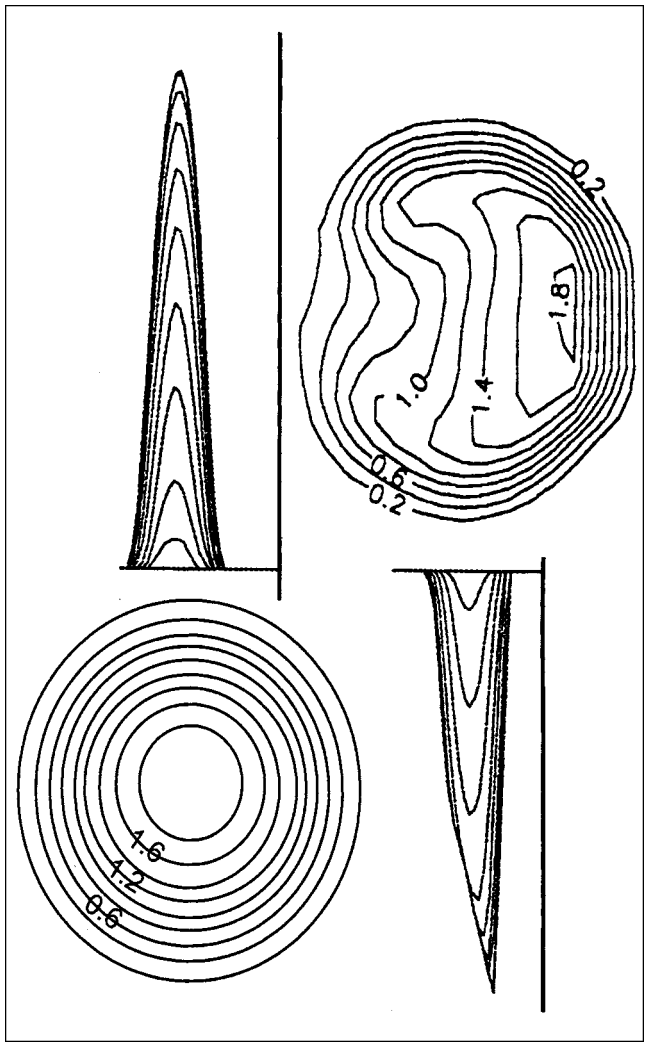

Figure 2. Typical MRFI results: surface and contour plots of axial or longitudinal velocities.

Flow entering the 180° curved section (left) is parabolic. Flow exiting the 180° curved section is squeezed to the outside (right) and contains Dean vortices.

The numerical techniques used in this study are available from a commercial computational fluid dynamics software package FLUENT (Fluent, Inc., 1993). Discretization and solution methods are described in detail by Chung et al. (1993b).

A large number of numerical studies are available in literature on the subject of flow in curved ducts. Most use a half-grid, that is, they assume a central plane of symmetry (Collins and Dennis, 1975; Dennis and Ng, 1982; Daskopoulos and Lenhoff, 1989). This had the obvious advantage of halving the computational time. In this study, three types of computational grids were used and tested: (a) a pseudo-cylindrical half-tube grid with an artificial radius of 1/1,000 of the actual tube radius (to circumvent the singularity at the tube center); (b) a pseudo-cylindrical full-tube grid with an artificial radius of 1/1,000 of the actual tube radius; and (c) a rectangular grid for the full tube without symmetry planes. Since results with the second and the third grids were the most interesting and are reported herein, only they are shown in Figure 1. Effects of using different grids are discussed below. The respective computational grids are of the size: (a) $41\times21\times11$; (b) $41\times35\times11$; (c) $41\times21\times21$. All computations were carried out on RISC 6000 workstations. The tolerance level for convergence was set, as recommended, at 10^{-3} for flow variables. Generally, a solution was obtained within 200 iteration steps in approximately 1.0 CPU h. Since evidence of the laminarization effects of Dean vortices on turbulent flow is available (Narasimha and Sreenivasan, 1979; Sreenivasan and Strykowski, 1983), simulations were carried out for Reynolds numbers up to the onset of turbulent flow in a curved tube.

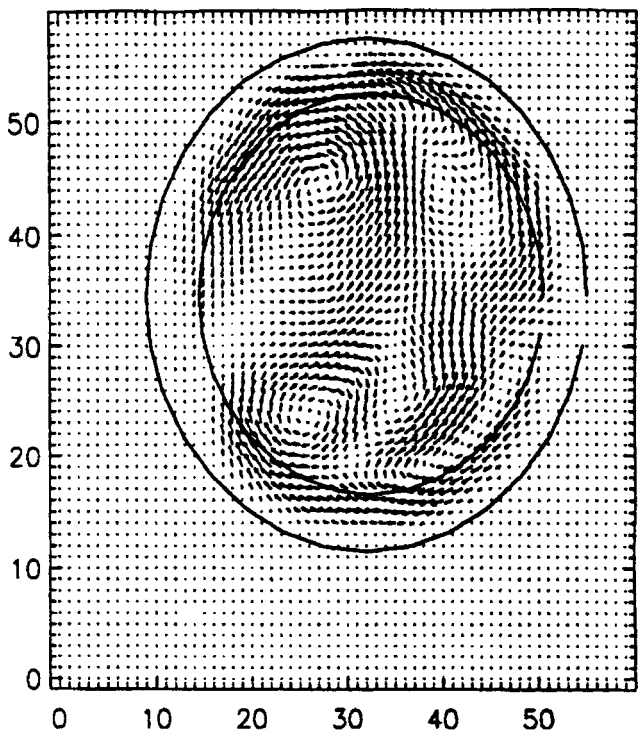

Figure 3. Typical MRFI results: Vector plot of the transverse velocities.

Each vector represents the local transverse velocity. Size of the vector is proportional to the transverse velocity magnitude.

Experimental Studies

The flow system was described in detail by Chung (1992) and Chung et al., (1993b). A 3-D pulse sequence described in detail by Chung et al. (1993b) was used to obtain the longitudinal, as well as the transverse, velocities for a slice starting from the end of the curved section and 12 mm thick. The spatial and velocity resolutions of this system were approximately 60 μm and 0.1 cm/s.

After calibrating the system for flow (Chung et al., 1993b), MRFI data were collected as a function of increasing flow rate for five tubes. The dimensions of these tubes are shown in Table 1. Run time for these experiments was approximately 45 min for each directional velocity. Experiments were repeated up to 9 times to confirm the patterns observed. The largest experimental error was about $\pm 4\%$ for transverse velocities (smaller the velocity, larger the error). For parabolic profiles in the linear tube, the error was lower than $\pm 0.5\%$. *Curved* longitudinal velocities showed an error of about $\pm 1\%$.

Although bifurcations/twisting were found for flow in curved ducts of low radius ratios, it should be noted that, to our knowledge, no one has undertaken the study of Dean vortex flow in curved tubes of radius ratios as high as those employed in this study (up to $(a/r_c) = 0.317$). A direct and quantitative comparison to existing results was thus not possible. Others (Berger et al. (1983) gives a partial listing), have used optical and numerical methods to study flow in curved tubes for (a/R_c) values of up to 0.1. Qualitative arguments which support the results reported here are given with the description of the results.

Results and Discussion

Magnetic resonance flow imaging (MRFI)

Typical results are shown in Figure 2. The surface plots show the direction of the distortion effect of the centrifugal force on the parabolic profile for laminar flow. Each contour is a locus of points (elements) of equal velocity. A set of contours gives the velocity profile. The contour plots show that for flow around a curve, the concentric circular contours of the regular parabolic profile are twisted into bean-shaped curves. The outer circle shown in Figure 3 (for transverse velocities) represents the wall of the glass U-tube. The inner circle is drawn arbitrarily (about 20% of the radius); the shear rates are estimated in the annular region formed by the two circles and the average of these shear rates is termed the

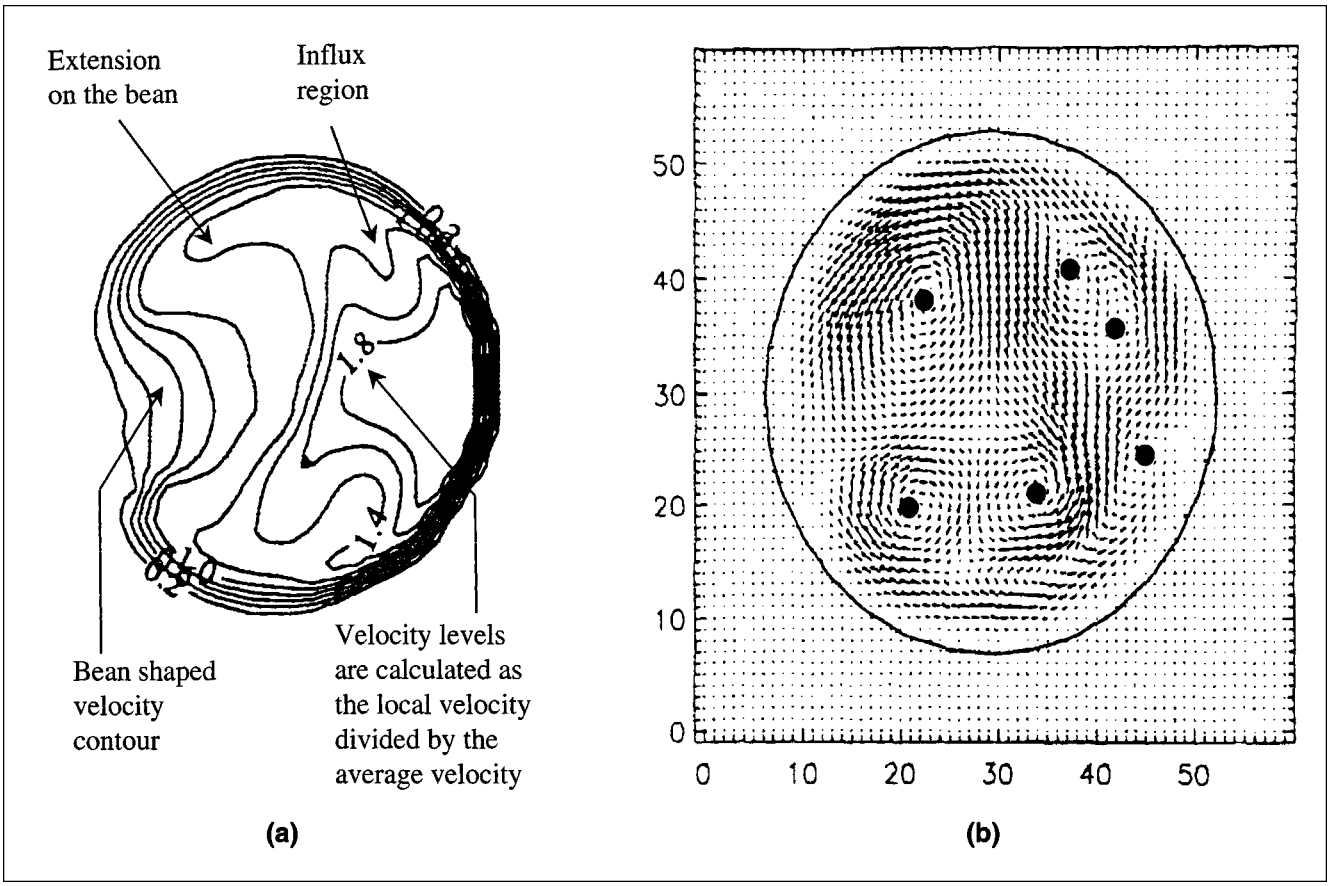

Figure 4. Typical MRFI results: How to *read* the figures in this article.

Pixel numbers depend on the block size. Actual tube dimensions are given in Table 1. (a) Contours of axial velocities as a fraction of the average axial fluid velocity; (b) transverse velocity vectors (arrows) in the transverse plane with the centrifugal force acting from left to right. Primary vortices are on the left. Visualizing the *eyes of the vortices* (·) helps *see* all the vortices. Secondary vortices on the right appear after bifurcation.

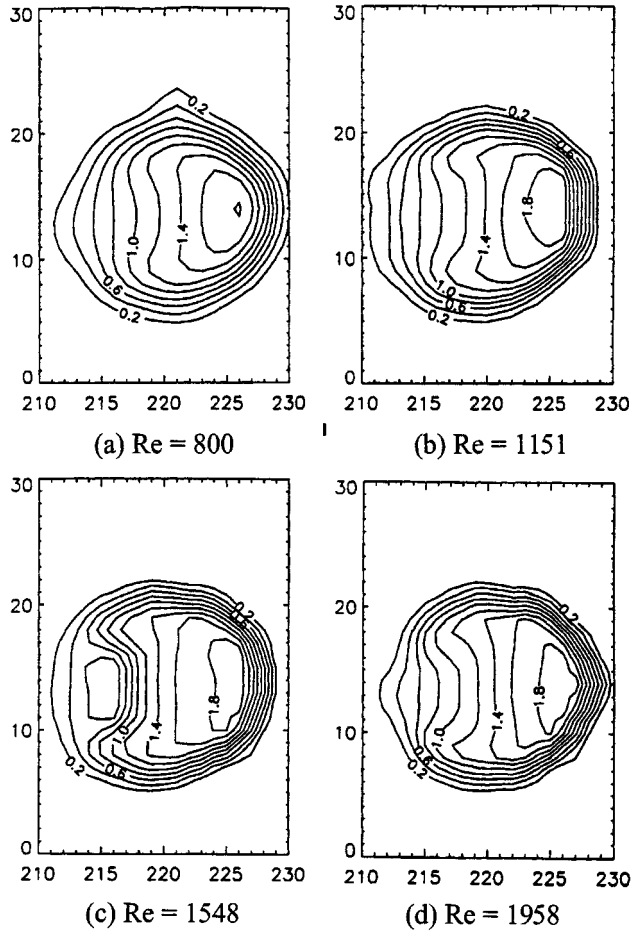

Figure 5. MRFI measurements.

Effect of increasing flow rate on the axial velocity contours for flow in a curved tube of radius ratio $(a/r_c) = 0.084$. The Dean numbers corresponding to the Reynolds numbers shown in the figure are (a) 249, (b) 443, (c) 648, and (d) 865.

transverse wall shear rate. The shear rates are calculated as

$$\gamma_t = \sqrt{\gamma_x^2 + \gamma_y^2} \tag{1}$$

Values of γ_x and γ_y are the average of 15 sets of points each taken at positions equally spaced around the circumference. Figures 4a and 4b show *how to read* the figures presented in this paper.

Figure 5 shows the effect of increasing flow rate on the axial or longitudinal velocity contours (normalized by the average velocity) for a tube of radius ratio, (a/r_C) of 0.084. Unless otherwise stated, levels shown in all the contour plots in this study are 0.2, 0.4, 0.6, 0.8, 1.0, 1.2, 1.4, 1.6, and 1.8 times the average velocity. With increasing flow rate, the distortion of the contours increased. At and above a Reynolds number of 1,548, the bean-shaped contours show extensions at the top and bottom ends of the bean. Such distortion increased with increasing flow rate and was highest for a Reynolds number of 2237 (data not shown). Above this flow rate, the contours became less distorted and in the so-called *transition regime*, regained their original shape.

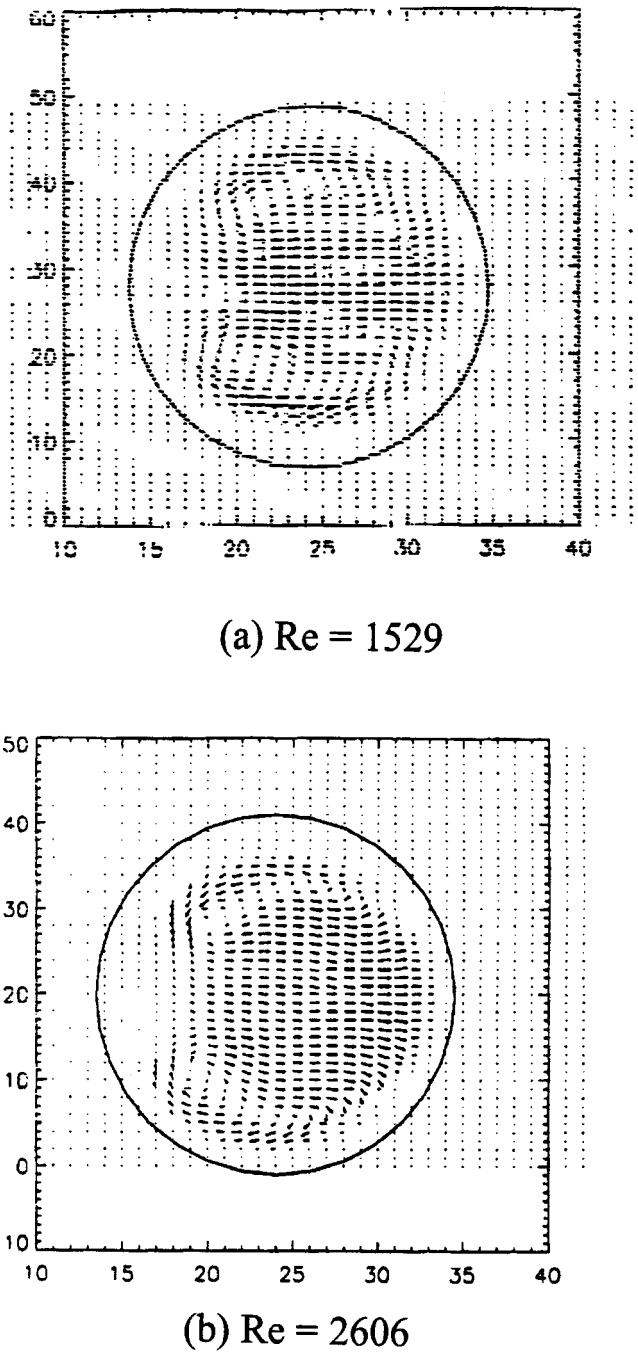

Figure 6. MRFI measurements.

Effect of increasing flow rate on the transverse velocities for flow in a curved tube of radius ratio $(a/r_c) = 0.084$. The Dean numbers corresponding to the Reynolds numbers shown in the figure are (a) 443 and (b) 755.

Transverse velocity data, collected at nearly corresponding Reynolds numbers, are shown in Figure 6. With increasing flow rate, the (eyes of the) vortices twist *toward* the central plane, in order to *counter-balance* the centrifugal force, which is highest at the central plane (Figure 6a). Note that this twisting behavior corresponds to the extensions of the bean-shaped contours at the top and bottom (for example, com-

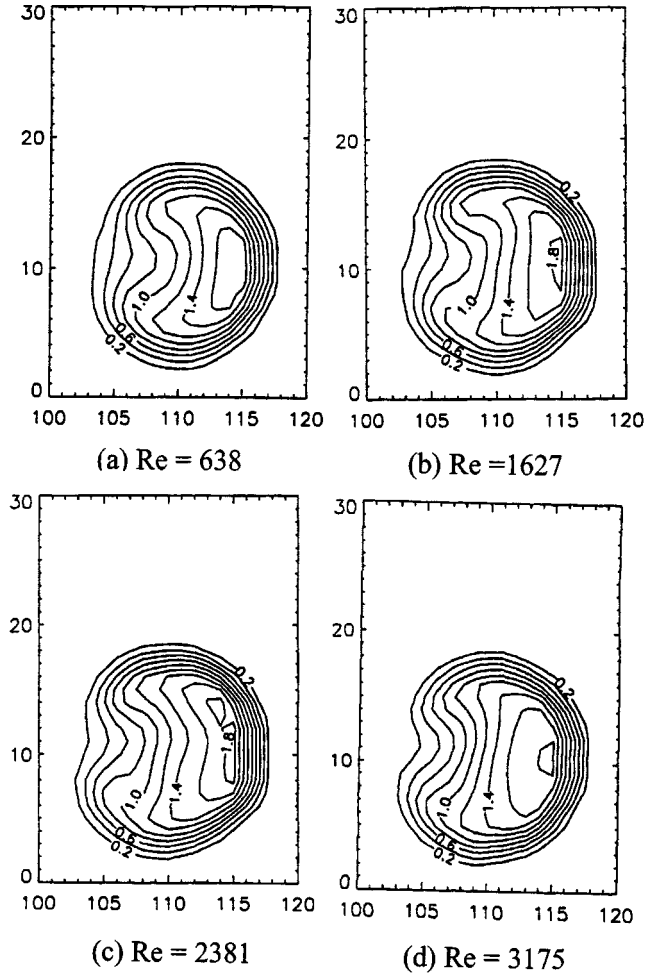

Figure 7. MRFI measurements.

Effect of increasing flow rate on the axial velocity contours for flow in a curved tube of radius ratio (a/r_c) = 0.154. The Dean numbers corresponding to the Reynolds numbers shown in the figure are (a) 250, (b) 637, (c) 932, and (d) 1244.

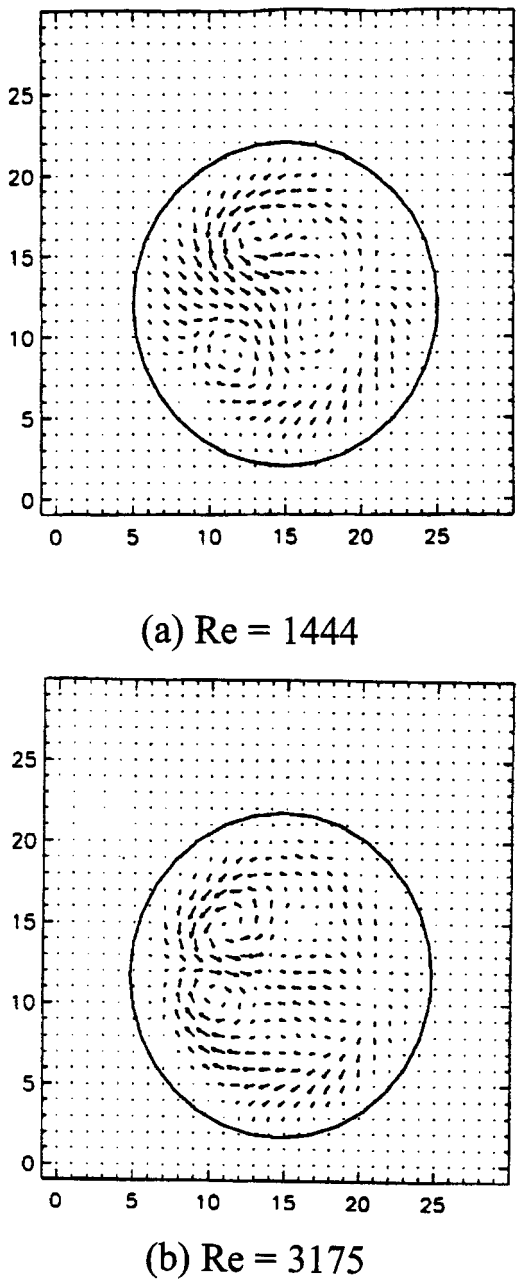

Figure 8. MRFI measurements.

Effect of increasing flow rate on the transverse velocities for flow in a curved tube of radius ratio (a/r_c) = 0.154. The Dean numbers corresponding to the Reynolds numbers shown in the figure are (a) 566 and (b) 1,244.

pare Figure 5c and Figure 9a). The vortices appear to bifurcate (that is, break-up into multiple vortices) completely at a Reynolds number of 2606, but with increasing flow rate (Re = 2983), the original pattern begins to re-establish itself (data not shown).

Figure 7 and Figure 8 show the effect of increasing flow rate on the axial velocity contours and transverse vectors, respectively, for a tube of radius ratio 0.154. For this radius ratio, the axial velocity contours show the extensions at a much lower Reynolds number (Figure 7a). In addition, the contours begin twisting clockwise. Above a Reynolds number of 1,627, the extensions at the top and bottom of the bean-shaped curves do not match (Figure 7b). In the transition regime ($Re > 2{,}381$), the original pattern seems to establish itself again (compare Figure 7a with Figure 7d). At a Reynolds number of 1,444, the transverse vectors show a small bifurcation in the lower vortex (Figure 8a). This bifurcation probably caused the dissimilar extensions observed in Figure 7b. Note that the upper vortex in Figure 8a is of greater strength (larger vectors). This shows that the strength of the vortices and the corresponding shear rate and cleaning ability of the vortices during filtration *decreases* with bifurcation. The bifurcated vortices gather strength with increasing flow rate, but further increase in flow rate seems to force the vortices to merge back. In the transition regime, although there is a significant amount of twisting, only two vortices are seen clearly (Figure 8b).

Dual solutions for flow in curved ducts are available in literature (Dennis and Ng, 1982). Yanase et al. (1989) found the existence of a three-vortex pattern.

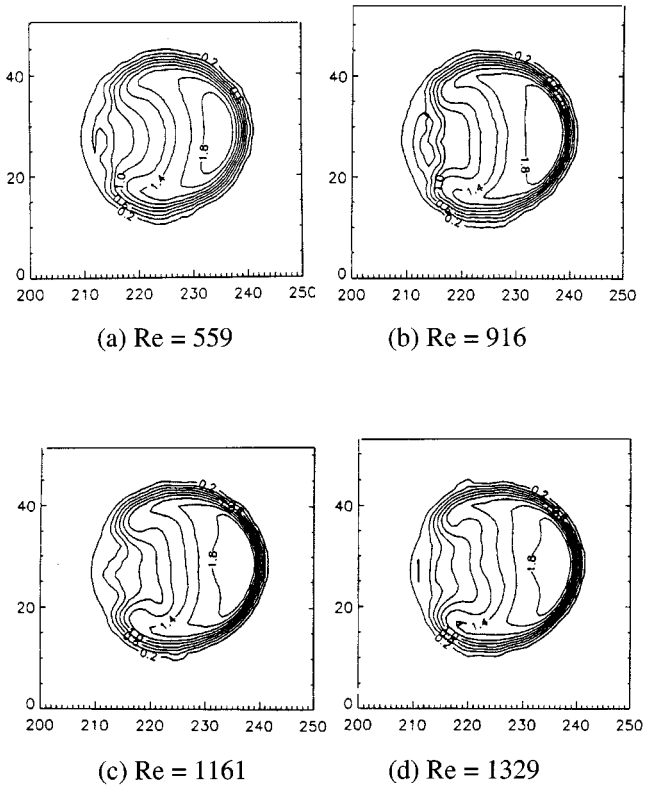

Figure 9. MRFI measurements.

Effect of increasing flow rate on the axial velocity contours for flow in a curved tube of radius ratio (a/r_c) = 0.192. The Dean numbers corresponding to the Reynolds numbers shown in the figure are (a) 245, (b) 401, (c) 508, and (d) 582.

Figures 9 and 10 show the effect of increasing flow rate on the axial velocity contours and transverse velocity vectors, respectively, for flow in a tube of radius ratio 0.192. With increased tube diameter, the scatter in the collected data increased. Since these are time-averaged results, this scatter is attributed to small disturbances in the fluid flow, due to pump vibrations and other factors. Such scatter is amplified by low velocities (an obvious effect of increased diameter for the same flow rate), since a low velocity would result in a lower signal.

The axial velocity contours for a radius ratio of 0.192 are more symmetrical about the central plane than those at the lower radius ratio of 0.154, although the extensions at the extremes of the bean-shaped curves appear at lower Reynolds numbers. At higher Reynolds numbers, these extensions were distorted further and showed clear points of inflection, suggesting a reverse flux of the fluid at these places (see level 1.2 in Figures 9c and 9d). Bifurcation begins to appear at a Reynolds number of 529 (data not shown), although it is not completely established until the Reynolds number is increased to 1,029 [as $De = Re\,(a/r_C)^{1/2}$]. Corresponding to the large distortions in the extensions of the bean-shaped curves, the transverse velocity vectors show further breakdown of the vortices. This breakdown has become more prominent as the Reynolds number is increased to 1,537 (Figure 10b). At the higher Reynolds number of 1,823, however, some order is restored (data not shown).

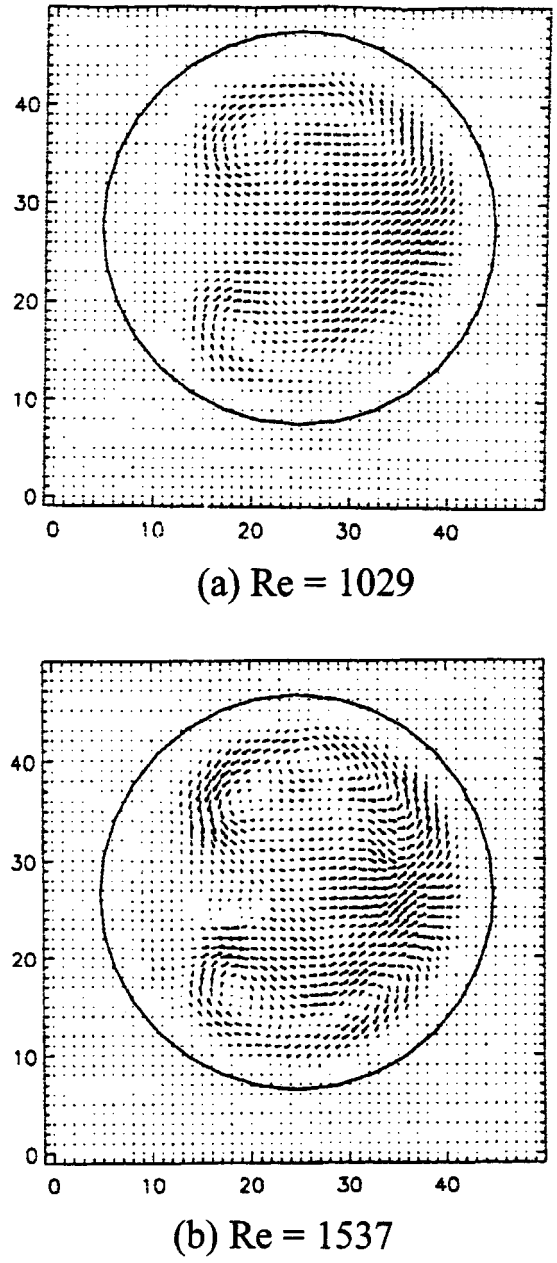

Figure 10. MRFI measurements.

Effect of increasing flow rate on the transverse velocities for flow in a curved tube of radius ratio (a/r_c) = 0.192. The Dean numbers corresponding to the Reynolds numbers shown in the figure are (a) 451 and (b) 673.

For the same average fluid velocity, it has been shown that the loss in signal due to turbulence was higher for a larger tube than for a smaller tube (Kuethe and Gao, 1995). Alternatively, signal loss increases with increasing *Re*. While this may partially explain the twisting behavior for smaller tube diameters and the bifurcation behavior for the larger tube diameters, it should be noted that a large number of scans were performed to minimize the loss in signal.

Figures 11 and 12 show the results for flow in a tube of a smaller diameter, but of a larger radius ratio (0.2575). The twisting of the axial velocity contours is significant even at

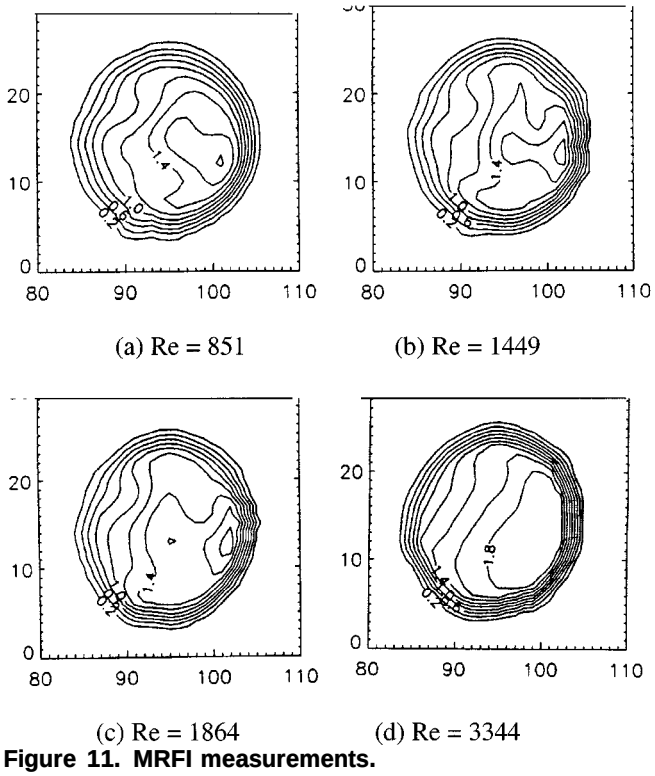

Figure 11. MRFI measurements.

Effect of increasing flow rate on the axial velocity contours for flow in a curved tube of radius ratio $(a/r_c) = 0.258$. The Dean numbers corresponding to the Reynolds numbers shown in the figure are (a) 432, (b) 735, (c) 946, and (d) 1697.

low Reynolds numbers. The bean-shaped curves are severely distorted above a Reynolds number of 851. These distortions increase with increasing flow rate (Figure 11b). With a further increase in Reynolds number, the high velocity contours (levels 1.6 and above), separate into two (Figure 11c). At higher Reynolds numbers, however, order is restored, although it appears that the distribution of the contours shows some kind of an oscillation of the high velocity contours. Also, the contours are twisted clockwise for all the higher flow rates.

The transverse velocity vector plots correspond to the twisting behavior of the axial velocity contours (Figure 12). At low flow rates, the pattern is the standard double vortex, while at higher flow rates, a large amount of twisting and bifurcation is observed. At a Reynolds number of 754, only three vortices are observed (Figure 12a). With increasing flow rate, these distortions gather strength and, at a Reynolds number of 1,758, they begin to merge (Figure 12b). With a further increase in Reynolds number, the vortex-doublet begins to reappear, although the plane that separates the two vortices is at an angle to the horizontal (data not shown).

Results of the tube with the highest radius ratio tested (0.317) are shown in Figures 13 and 14. Note that the diameter of this tube is also large (2a = 16.04 mm). At low Reynolds numbers, the standard bean-shaped curves are seen, while at higher flow rates, these curves developed extensions at the top and bottom as discussed before. A significant difference is the protrusion in the middle of these contours, opposite to the direction of the centrifugal force (see level 1.2 in Figure

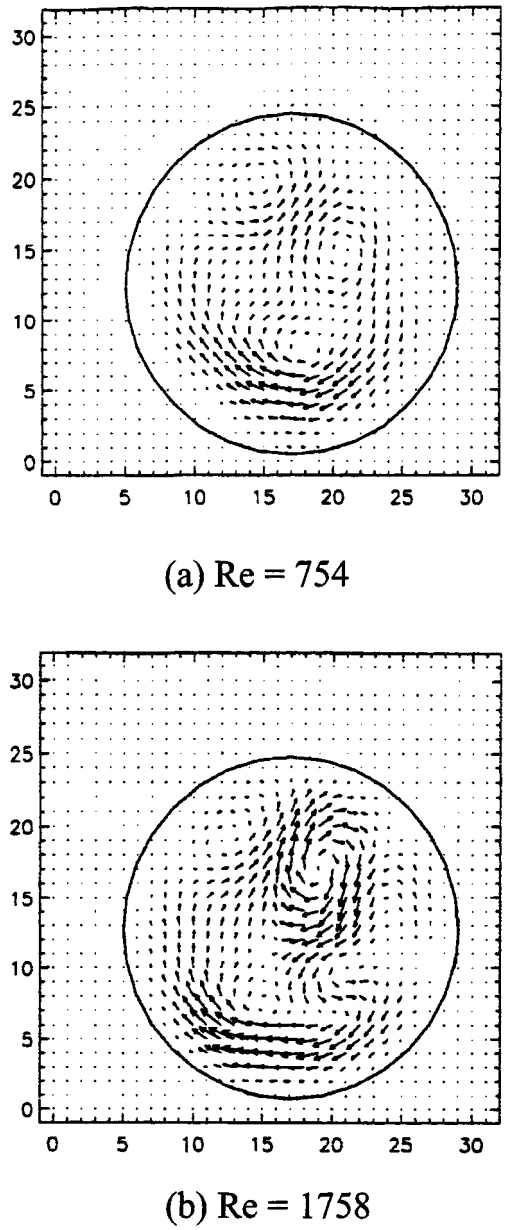

Figure 12. MRFI measurements.

Effect of increasing flow rate on the transverse velocities for flow in a curved tube of radius ratio $(a/r_c) = 0.258$. The Dean numbers corresponding to the Reynolds numbers shown in the figure are (a) 383 and (b) 892.

13a). At higher flow rates, the higher contours develop influx regions (see level 1.4 in Figure 13b). This suggests that the flow is separating into two regions moving away from each other. This behavior becomes more pronounced at higher flow rates. The transition regime was not reached with this tube because of pump limitations. Even at a Reynolds number of 1,949, the patterns with the influx regions remained. The area of the highest contour (level 1.8), increased with increasing *Re* (Figure 13d).

The longitudinal velocity contours retained a higher degree of symmetry about the central plane at this radius ratio (0.317), than at the lower radius ratio of 0.258. The degree of

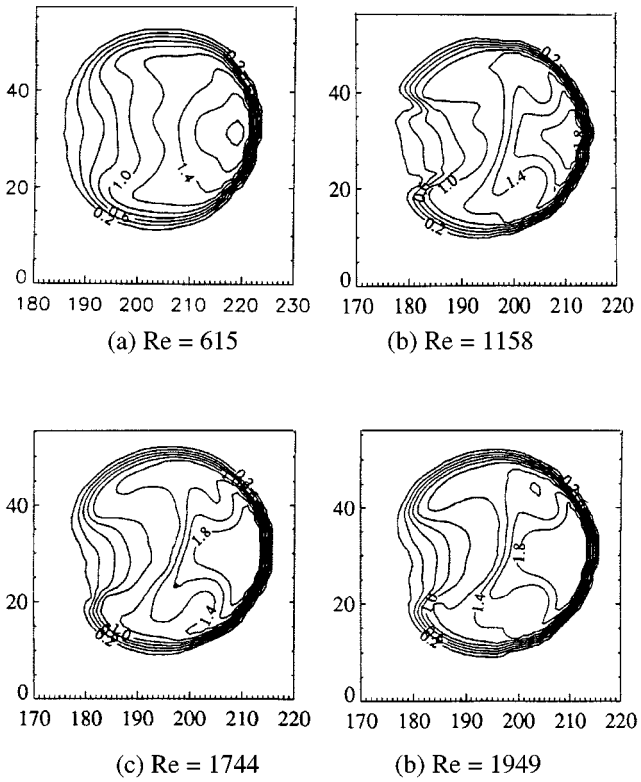

Figure 13. MRFI measurements.

Effect of increasing flow rate on the axial velocity contours for flow in a curved tube of radius ratio (a/r_c) = 0.317. The Dean numbers corresponding to the Reynolds numbers shown in the figure are (a) 346, (b) 652, (c) 982, and (d) 1,098.

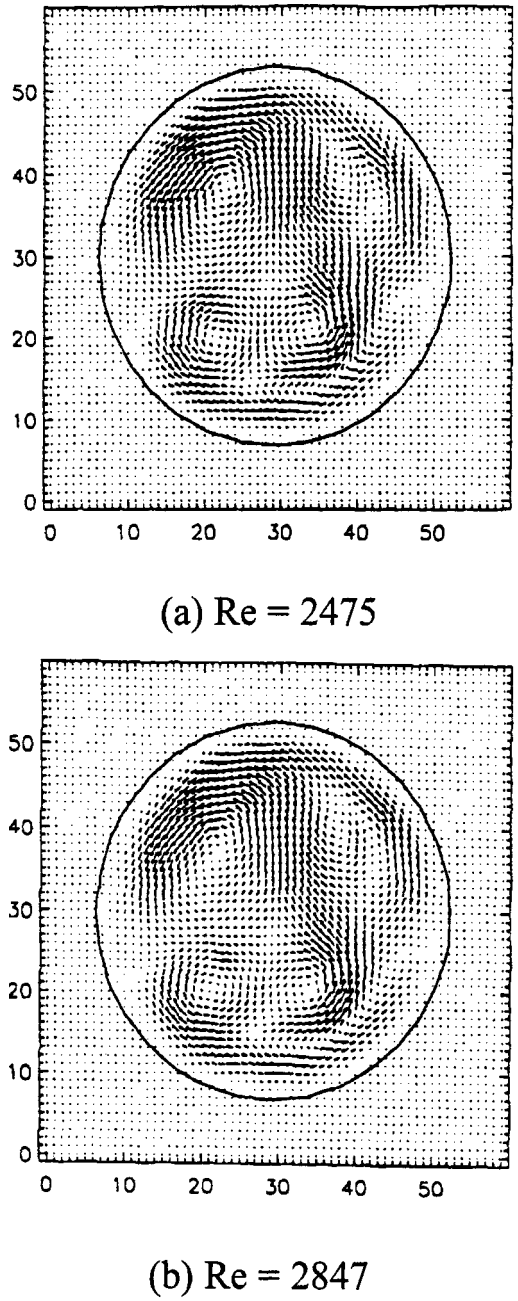

Figure 14. MRFI measurements.

Effect of increasing flow rate on the transverse velocities for flow in a curved tube of radius ratio (a/r_c) = 0.317. The Dean numbers corresponding to the Reynolds numbers shown in the figure are (a) 987 and (b) 1,102.

symmetry was higher for the radius ratio of 0.192 than at 0.258 (compare Figure 9 with Figure 11). This suggests that both the tube radius, as well as the radius ratio, affect Dean vortex flow. Alternatively, the Dean number itself does not appear to encompass the effects of the channel geometry. It appears that for smaller tube radii, the flow is *restricted* from bifurcating. This results in the twisting of the vortex patterns. For larger tube radii, the twisting is reduced, because the fluid elements have more *freedom* for movement. This seems reasonable, because at the same Reynolds or Dean number, the fluid-velocities in the larger tube are smaller compared to those in the smaller tube. For lower velocities in the smaller tube, the Dean number is small and therefore there is no twisting or bifurcation. Numerical evidence for the additional effect of the radius ratio in improving heat transfer is available in literature (Mori and Nakayama, 1965).

The transverse velocity plots for corresponding Reynolds numbers show that the bifurcation/twisting begins at low Reynolds numbers. Corresponding to the *influx* regions discussed above for axial velocity contours, the vortex pattern bifurcates into six vortices (compare Figure 13c with Figure 14a and Figure 13d with Figure 14b). In Figure 14a, the two primary vortices occupy almost half of the tube and move *toward* the central plane (where the centrifugal force is the highest) and *against* the direction of the centrifugal force. The remaining four vortices appear to cause the *influx* regions, where the flow is separating into two regions moving away from each other. The vortices thus appear to twist or bifurcate such that they move to *counterbalance* the centrifugal force along the central plane. This is similar to the effect of torsion on the vortices in a helical tube (the vortices twist against the torsion) (Liu and Masliyah, 1993; Chen and Jan, 1992). Splitting and merging events for Dean vortex flow in curved slit channels have been verified by several researchers (Bottaro et al., 1991; Matsson and Alfredsson, 1992; Ligrani

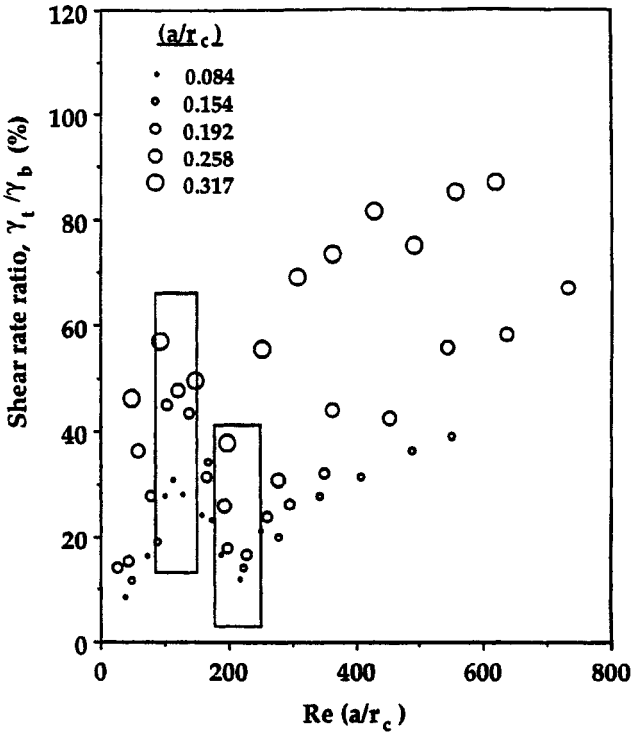

Figure 15. Effect of $Re(a/r_c)$ on normalized transverse shear rates taken from MRFI measurements.

The radius ratio (a/r_c) increases with the size of the symbol.

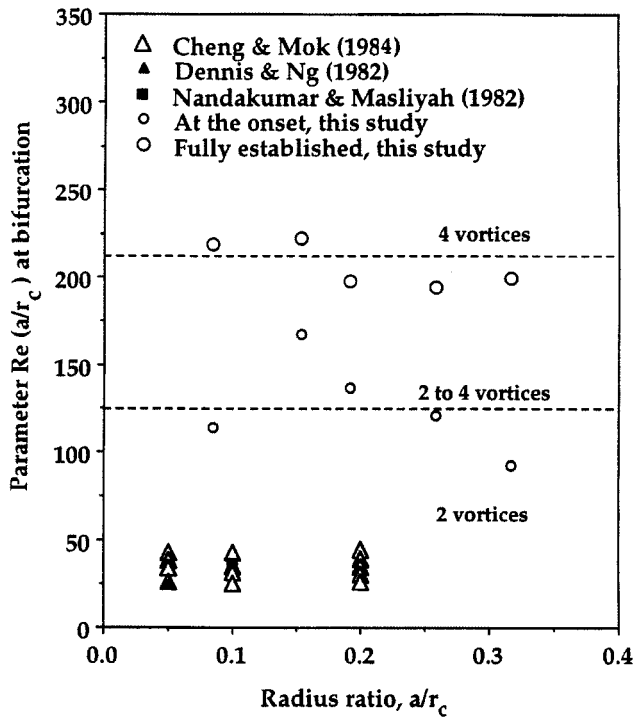

Figure 16. Effect of radius ratio (a/r_c) on the parameter $Re(a/r_c)$ taken from MRFI measurements.

Values at the onset of the bifurcation of the Dean vortex doublet and for the fully established four-vortex pattern are shown.

et al., 1994). With increasing *Re*, the vortices split and at higher *Re* they merge. 2-D multiple solutions were found numerically and confirmed experimentally for flow in a curved duct of square cross-section (Bara et al., 1992). Mees et al. (1996a,b) have found a six-vortex pattern for the case of a square cross-section.

Cheng and Mok (1984) suggested that at the bifurcation, the parameter $Re(a/r_c)$, remains constant. They also report a value of about 37 for the parameter $Re(a/r_c)$ at the onset of the four-vortex instability. Average wall shear rates normalized with the shear rate due to axial velocity for laminar flow in a tube are plotted against this parameter in Figure 15. With increasing flow rate, the shear rates induced by Dean vortices increased, but as the vortices twisted or bifurcated, the shear rate ratio dropped, followed by further increase in shear rate ratio. This behavior was observed for all tubes. It is also observed that the shear rate ratio increased with increasing radius ratio. The shear rate minima were observed at about a value of 212 for the parameter $Re(a/r_c)$, which corresponds with the fully established four-vortex pattern for all the tubes, while the maxima are at about a value of 125 for the parameter $Re(a/r_c)$. Data below the shear rate maxima had only two vortex patterns, while those between the maxima and the minima showed the change from two to four vortices. Figure 16 shows the values of this parameter at the bifurcation as a function of radius ratio. Data from literature are also shown (Dennis and Ng, 1982; Cheng and Mok, 1984; Nandakumar and Masliyah, 1982).

Cheng and Mok (1984), however, report that the uncertainty in determining the onset of this instability, using optical methods, is about 100% of the Dean number at the onset of the four-vortex pattern. The large difference between the observed values (ranging from 90 to 175, with an average of about 125, vs. 37 ± 37) of the parameter $Re(a/r_c)$ is probably due to the different methods of observation. They have used an invasive method, which consists of the insertion of a needle at the exit of the curved bend, while MRFI is noninvasive. Cheng and Mok (1984) also comment that the Dean vortices disappear above a Dean number of 1,000. As shown here, Dean vortices exist at least up to a Dean number of 1836.

Numerical predictions

Numerical studies in the literature report the first occurrence of the bifurcation at Dean numbers much higher than those observed experimentally. The general method to obtain the bifurcation is to solve the governing equations starting from the lowest Dean number and use the solution as an initial guess for the next *higher* Dean number, until a bifurcation is observed. The solution containing the bifurcation is then used as an initial guess to solve the equations at the next *lower* Dean number, and so on, until the lowest Dean number is reached (Yanase et al., 1989). This upper hysteresis curve is claimed to correspond to the experimental observations and is explained by Benjamin's (1978a,b) theory of bifurcation, which states that a bifurcation should be approached *from the top*, that is, by decreasing the flow rate. For all the grids used in this study, solutions were obtained at various Dean or Reynolds numbers, while increasing as well decreasing, the flow rate.

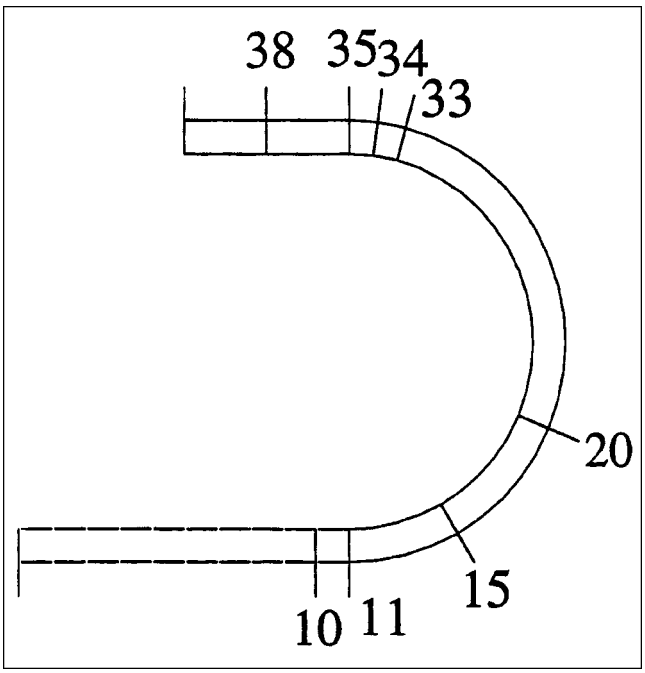

Figure 17. Slice selection for the numerical analysis.

Fluid entering slice 10 has a nearly parabolic profile. Results at slice 38 (12 mm from the end of the curved section) are compared to those of the MRFI.

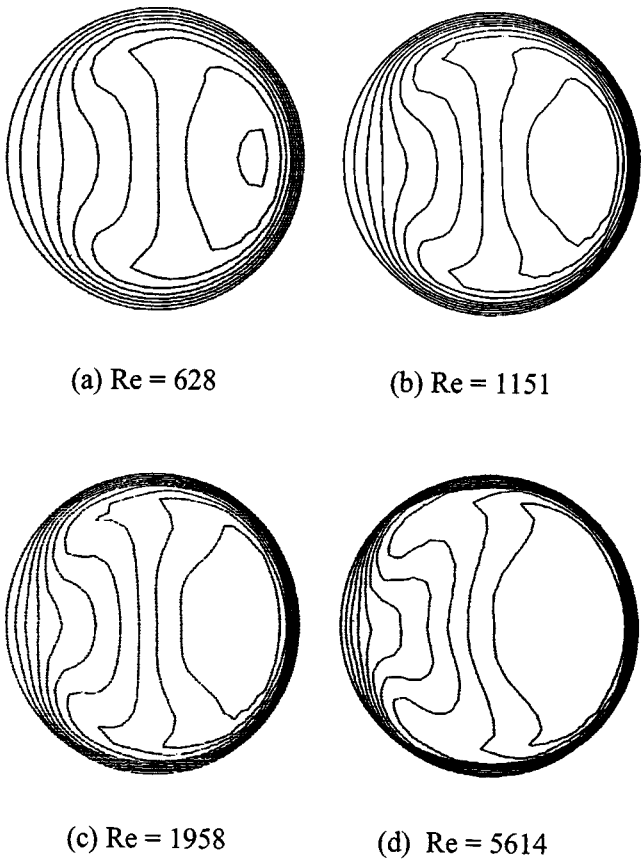

Figure 18. Numerical results with the full-grid without planes of symmetry showing the axial velocity contours.

Effect of increasing flow rate on the axial velocity contours for flow in a curved tube of radius ratio $(a/r_c) = 0.317$. The Dean numbers corresponding to the Reynolds numbers shown in the figure are (a) 346 and (b) 982.

For proper comparison with the MRFI data, it should be noted that the numerical solution data at the slice immediately after the curved section (slice no. 35 in Figure 17) should not be used. The appropriate slice is further downstream. This is because of the finite thickness of the MRFI slice (12 mm thick and extends from the end of the *curved* section). Axial velocity contour, transverse velocity vector, and shear rate results from the appropriate slice are shown in this study.

Most solutions reported are based on the half-tube, since this saves computational time (Collins and Dennis, 1975; Dennis and Ng, 1982; Daskopoulos and Lenhoff, 1989; Chung et al., 1993b). Symmetry is assumed about the central plane (shown as a straight line in all the figures), and the equations are solved only for the half-tube. Mirror images of the solution are put together to obtain the complete solution. Although solutions for the half-grid and full-grid gave qualitatively good results, the velocity profiles were disturbed because of the singularity at the center. No large distortions were found in the contours and very high Reynolds numbers were required to produce four- and six-vortex patterns.

Figures 18 and 19 show the results for the grid without symmetry planes. Velocity levels 0, 0.2, 0.4, 0.6, 0.8, 1.0, 1.2, 1.4, 1.6, and 1.8 are shown for the axial velocity contours. With increasing flow rate, results from this grid show the extensions at the top and bottom of the bean-shaped curves even at low flow rates (compare Figure 13a with Figure 18a). The influx regions, on the other hand, are not as clearly established, although a hint of the development can be seen in Figure 18b (compare with Figure 16b). Even a slight dissimilarity is produced at the top and bottom of the contours. The area of the highest level contour (velocity 1.8 times the mean) increased with increasing Reynolds number. A similar trend was observed experimentally. At higher Reynolds numbers, the extensions at the top and bottom of the curves increased and resembled those observed experimentally at lower flow rates (see Figures 18d and 16d). The results compare very well, quantitatively, with those observed experimentally at low flow rates. However, the results are only slightly better than those from the other two grids at higher flow rates, especially after the six-vortex pattern is established.

Figure 19 shows the transverse velocity plots with increasing Reynolds number. A bifurcation is seen clearly even at low flow rates (Figure 19a), and, at high flow rates, the six-vortex pattern is clearly seen (Figure 19b). The primary vortices are seen to occupy almost half the tube as was observed experimentally. Also, the vortex patterns match with those observed experimentally (compare Figure 14a with Figure 19b).

Friction factors calculated from the axial pressure drop data are shown in Figure 20. Note that the critical Reynolds number (that is, the Reynolds number above which the Dean vortices are thought to be present and significant) for this radius ratio (0.317) was calculated to be 31.7 using the wide-gap theory (Brewster et al., 1993). The curved friction factor appears to separate from the Hagen-Poiseuille equation for straight

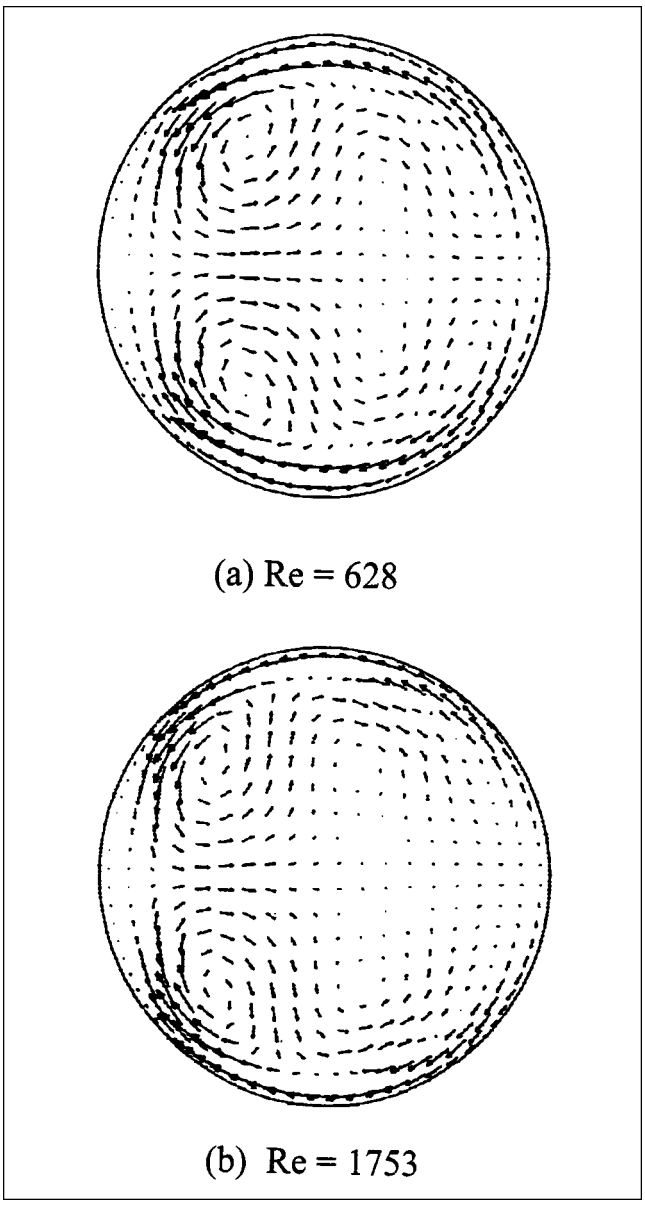

Figure 19. Numerical results with the full-grid without planes of symmetry showing the transverse velocity vectors (arrows).

Effect of increasing flow rate on the transverse velocities for flow in a curved tube of radius ratio $(a/r_c) = 0.317$. The Dean numbers corresponding to the Reynolds numbers shown in the figure are (a) 346 and (b) 982.

tubes above this Reynolds number, imparting credence to the hypothesis that the wide-gap theory developed for flow in curved slits can be used to calculate the critical Reynolds number for flow in curved tubes. Also, the friction factors calculated from the numerical axial pressure drop data for the full-grid with a plane of symmetry showed a mild hysteresis close to the critical Reynolds number (Figure 20a). With decreasing *Re*, the friction factor curve for flow in a curved tube approached the line for friction factor in straight tubes, as the Reynolds number approached the critical value of 31.7. Friction factors calculated from the axial pressure drop data for a full-grid without a plane of symmetry are shown in Figure 20b. These calculated data do not exhibit any hysteresis. Figure 21 shows the comparison of the calculated transverse shear rate results with experimental MRFI results for the full-grid with and without a central plane of symmetry. Although there is some agreement between the numerical and experimental results, the numerical results suggest that the shear rate induced by Dean vortex flow increased monotonically with increasing flow rate. For the case with a full grid and a plane of symmetry (Figure 21a), the numerical predictions are close to the MRFI measurements. They do not, however, track the subtle changes in transverse shear rate with increasing Reynolds number. For a full-grid without a plane of symmetry, the numerical and MRFI experimental results diverge above a *Re* of about 1,000 (Figure 21b). No hysteresis was observed for the transverse shear rate with increasing and decreasing flow rate (*Re*) for the occurrence of the bifurcation.

Conclusions

Velocity profiles for flow in curved tubes were measured using nuclear magnetic resonance flow imaging. Numerical solutions of the Navier-Stokes equations were obtained with a finite volume method to approximate the experimental results. The main conclusions are:

(1) Axial and transverse velocities during flow in curved tubes of various radius ratios were measured using MRFI, as a function of increasing *Re*. Correspondence between axial and transverse velocities in terms of twisting and bifurcation was obtained (see (4) below).

(2) Morphogenesis of the twisting and bifurcation of Dean vortices were measured. With increasing flow rate, the vortices were found to twist against the centrifugal force. Primary vortices were also found to move against the centrifugal force. At similar Dean numbers, twisting was found to be more prevalent in tubes of smaller diameter, while bifurcation of the vortices was more extensive in tubes of larger diameter. On the other hand, twisting and/or bifurcation occurred at lower flow rates as the radius ratio increased.

(3) The twisting/bifurcation increased with increasing flow rate. At least for tubes of smaller diameter, the twisting/bifurcation decreased in the transition regime and vortex patterns similar to those at low flow rates were re-established.

(4) Bifurcation of the standard vortex doublet, to four and then to six vortices, was obtained for the tube of the highest radius ratio (0.317). Axial velocity profiles at these flow rates showed influx regions, that is, velocity contours moved in opposite directions.

(5) The parameter $Re\,(a/r_c)$ for the flow rate at which the four-vortex pattern was fully established was found to be nearly constant for all the radius ratios. The same parameter at the onset of the four-vortex instability showed greater variation. Both these values were much higher than those reported in literature.

(6) Wall shear rates were estimated from transverse velocity measurements. These shear rates increased with increasing flow rate, passed through a maximum, decreased to a minimum, and then increased. The maxima corresponded to the onset of twisting/bifurcation to the four-vortex pattern, and the minima corresponded to the fully established four-

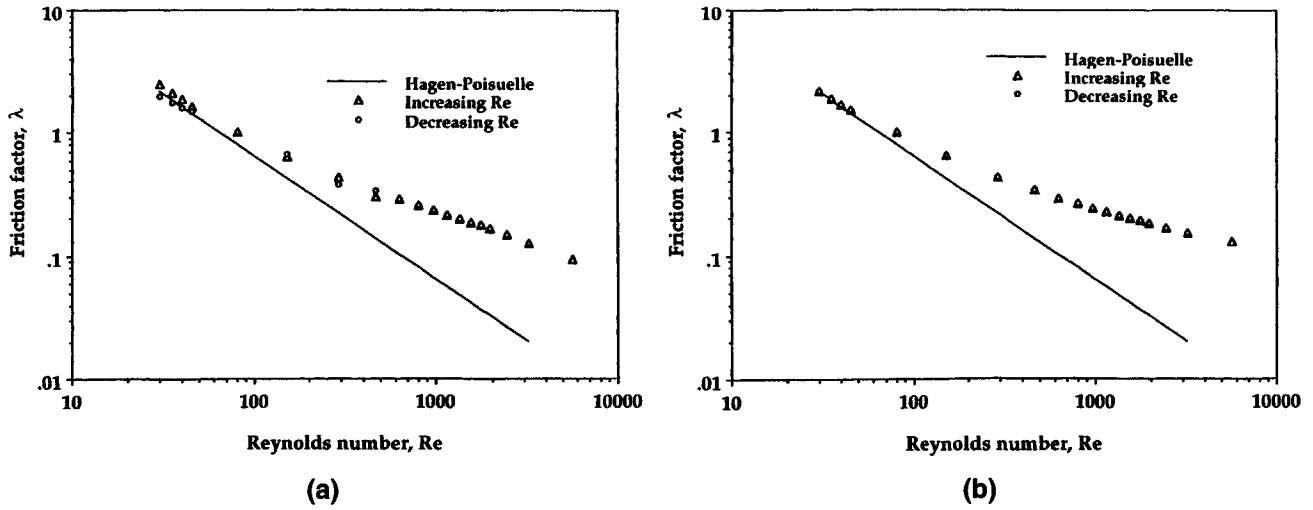

Figure 20. Results with the full-grid (a) with and (b) without planes of symmetry.

Calculated friction factors as a function of Reynolds numbers. The curves diverge significantly from the Hagen-Poiseuille equation above the critical Reynolds number of 31.7.

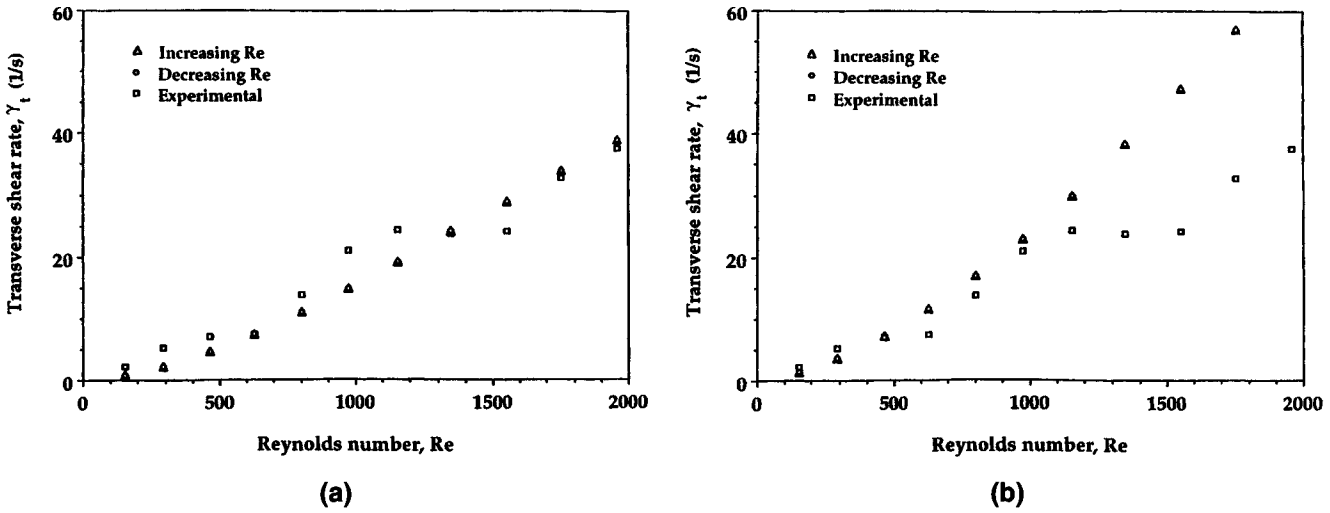

Figure 21. Results with the full-grid (a) with and (b) without planes of symmetry.

Comparison of numerical transverse shear rates with those obtained experimentally.

vortex pattern. These results helped explain the results for microfiltration (Mallubhotla et al., 1995).

(7) Three types of finite-element grids were used to solve the Navier-Stokes equations for flow in a curved tube of radius ratio 0.317. These were: (a) a pseudo-cylindrical half-tube grid with a central symmetry plane; (b) a pseudo-cylindrical full-tube grid with a plane of symmetry; and (c) a full-tube grid without symmetry planes. Simulations were performed with increasing, as well as decreasing, Reynolds numbers. No significant hysteresis was found between simulations for the friction factor and the transverse shear rate with increasing and decreasing *Re*. This contradicts results reported in literature.

(8) Friction factors, calculated from numerical pressure drop data, support the hypothesis that the wide-gap theory developed for flow in curved slits can be used for flow in curved tubes to calculate the critical Reynolds number.

(9) Numerically obtained wall shear rates increased monotonically with increasing *Re*, as opposed to the wavy curve found experimentally using MRFI. Predictions for the transverse shear rate using the full-tube grid with a plane of symmetry were relatively good, while those for the full-tube grid without a plane of symmetry diverged from the MRFI data at Reynolds numbers greater than 1,000.

(10) Numerically obtained axial velocity contour profiles and transverse velocities were compared with those obtained experimentally by MRFI. The best agreement was found for the full-tube grid without symmetry planes. Influx regions for the axial velocity contours and the six-vortex pattern were obtained. Primary vortices were shown to move against the

centrifugal force, similar to the experimentally observed results. Twisting of the vortices was not observed for any of the grids.

Acknowledgments

The authors thank General Electric Company, Schenectady, NY, for the use of the nuclear magnetic resonance spectrometer, and Dr. Xianming Li, formerly of Fluent, Inc., Lebanon, NH, who initially helped with the numerical analysis. The National Water Research Institute partially funded this work.

This article No. 16 in the series on enhancement of membrane filtration performance due to secondary Dean flows. Part of the results were presented by G. Belfort as ''MRI and Numerical Analysis of Curved Tube Flows. Effect of Curvature on Dean Vortex Bifurcation,'' Paper No 31E, at the session in honor of Alan S. Michaels, AIChE Meeting, Dallas, TX (Nov. 1999).

Notation

(a/r_C) = ratio of tube radius to radius of curvature
a = inner radius of the hollow fiber, mm
De = Dean number, $De = Re\ (a/r_C)^{1/2}$
Q = flow rate (L/min)
r_C = center-line radius of curvature, mm
Re = Reynolds number, $Re = 2aV/\upsilon$
V = average velocity, m/s
ν = kinematic viscosity, m^2/s
γ = shear rate, L/s

Subscripts

b = bulk flow
t = transverse
x = x-direction
y = y-direction

Literature Cited

Bara, B., K. Nandakumar, and J. Masliyah, ''An Experimental and Numerical Study of the Dean Problem: Flow Development towards Two-Dimensional Multiple Solutions,'' *J. Fluid Mech.*, **244**, 339 (1992).

Battocletti, J. H., ''NMR Proton Imaging,'' *CRC Critical Rev. Biomed. Eng.*, **11**, 313 (1984).

Belfort, G., ''Fluid Mechanics in Membrane Filtration: Recent Developments,'' *J. Memb. Sci.*, **40**, 123 (1989).

Belfort, G., Coiled Membrane Filtration System, U.S. Patent No. 5,626,758 (1997).

Belfort, G., J. M. Pimbley, A. Greiner, and K-Y. Chung, ''Diagnosis of Membrane Fouling Using a Rotating Annular Filter, 1. Cell Culture Media,'' *J. Memb. Sci.*, **77**, 1 (1993a).

Belfort, G., P. Mikulasek, J. M. Pimbley, and K-Y. Chung, ''Diagnosis of Membrane Fouling Using a Rotating Annular Filter. 2. Dilute Particle Suspensions of Known Particle Size,'' *J. Memb. Sci.*, **77**, 23 (1993b).

Belfort, G., M. E. Brewster, and K-Y. Chung, Curved Channel Membrane Filtration, U.S. Patent No. 5,204,002 (1993c).

Benjamin, T. B., ''Bifurcation Phenomena in Steady Flows of a Viscous Fluid I. Theory,'' *Proc. R. Soc. Lond. A*, **359**, 1 (1978a).

Benjamin, T. B., ''Bifurcation Phenomena in Steady Flows of a Viscous Fluid II. Experiments,'' *Proc. R. Soc. Lond. A*, **359**, 27 (1978b).

Berger, S. A., L. Talbot, and L. S. Yao, ''Flow in Curved Pipes,'' *Ann. Rev. Fluid Mech.*, **15**, 461 (1983).

Bottaro, A. M., O. J. E. Matsson, and P. H. Alfredsson, ''Numerical and Experimental Results for Developing Curved Channel Flow,'' *Phys. Fluids*, **3**, 1473 (1991).

Bottomley, P. A., ''NMR Imaging Techniques and Applications: A Review,'' *Rev. Sci. Instrum.*, **59**, 1319 (1982).

Brewster, M. E., K-Y. Chung, and G. Belfort, ''Dean Vortices with Wall Flux in a Curved Channel Membrane System 1. A New Approach to Membrane Module Design,'' *J. Memb. Sci.*, **81**, 127 (1993).

Bubolz, M., M. Wille, G. Langer, and U. Werner, ''Beitrag zum Einflus von Deun-Wirbeln auf die Qufstromfiltration,'' *F and S Filtrieren und Separiereu*, **1**, 16 (1998).

Caprihan, A., and E. Fukushima, ''Flow Measurements by NMR,'' *Phys. Rep.*, **198**, 195 (1990).

Chen, W., and R. Jan, ''The Characteristics of Laminar Flow in a Helical Circular Pipe,'' *J. of Fluid Mech.*, **244**, 241 (1992).

Cheng, K. C., and S. Y. Mok, ''Flow Visualization Studies on Secondary Flow Patterns and Centrifugal Instability Phenomena in Curved Tubes,'' *Fluid Control and Measurement*, M. Harada, ed., Pergamon, Vol. 2, p. 765 (1984).

Chung, K-Y., ''Instabilities of Viscous Fluid Flow in a Curved Channel: A New Approach to Membrane Module Design,'' PhD Thesis, Rensselaer Polytechnic Inst., Troy, NY (1992).

Chung, K-Y., R. Bates, and G. Belfort, ''Dean Vortices with Wall Flux in a Curved Channel Membrane System. 4. Effect of Vortices on Permeation Fluxes of Suspensions in Microporous Membrane,'' *J. Memb. Sci.*, **81**, 139 (1993a).

Chung, K-Y., W. A. Edelstein, X. Li, and G. Belfort, ''Dean Vortices in a Curved Channel Membrane System: 5. Three Dimensional Magnetic Resonance Imaging and Numerical Analysis of the Velocity Field in a Curved Impermeable Tube,'' *AIChE J.*, **39**, 1592 (1993b).

Chung, K-Y., W. A. Edelstein, and G. Belfort, ''Dean Vortices with Wall Flux in a Curved Channel Membrane System: 6. Two Dimensional Magnetic Resonance Imaging of the Velocity Field in a Curved Impermeable Slit,'' *J. Memb. Sci.*, **81**, 151 (1993c).

Chung, K-Y., M. E. Brewster, and G. Belfort, ''Dean Vortices with Wall Flux in a Curved Channel Membrane System: 2. The Velocity Field, *AIChE J.*, **42**, 347 (1996).

Chung, K-Y., M. E. Brewster, and G. Belfort, ''Dean Vortices with Wall Flux in a Curved Channel Membrane System: 3. Concentration Polarization in a Spiral Reverse Osmosis Slit,'' *J. Chem. Eng. Japan*, **31**, 683 (1998).

Coles, D., ''Transition in Circular Couette Flow,'' *J. Fluid Mech.*, **21**, 385 (1965).

Collins, W. M., and S. C. R. Dennis, ''The Steady Motion of a Viscous Fluid in a Curved Tube,'' *Q. J. Mech. Appl. Math.*, **28**, 133 (1975).

Daskopoulos, P., and A. M. Lenhoff, ''Flow in Curved Ducts: Bifurcation Structure for Stationary Ducts,'' *J. Fluid Mech.*, **203**, 125 (1989).

Dennis, S. C. R., and M. Ng, ''Dual Solutions for Steady Laminar Flow through a Curved Tube,'' *Q. J. Mech. Appl. Math.*, **35**, 305 (1982).

Fluent, Inc., *FLUENT User's Manual*, Version 4.2, Lebanon, NH (1993).

Gehlert, G., S. Luque, and G. Belfort, ''Comparison of Ultra- and Microfiltration in the Presence and Absence of Secondary Flow with Polysaccharides, Proteins, and Yeast Suspensions,'' *Biotech. Prog.*, **14**, 931 (1998).

Hammer, B. E., C. A. Heath, S. D. Mirer, and G. Belfort, ''Quantitative Flow Measurements in Bioreactors by Nuclear Magnetic Resonance Imaging,'' *Bio/Tech.*, **8**, 327 (1990).

Heath, C. A., G. Belfort, B. E. Hammer, S. D. Mirer, and J. M. Pimbley, ''Magnetic Resonance Imaging and Modeling of Flow in Bioreactors,'' *AIChE J.*, **36**, 547 (1990).

Kelleher, M. D., D. L. Flentie, and R. J. McKee, ''An Experimental Study of the Secondary Flow in a Curved Rectangular Channel,'' *Trans. ASME*, **102**, 92 (1980).

Keulegan, G. H., and K. H. Beij, ''Pressure Losses for Fluid Flow in Curved Pipes,'' *J. Res. NBS*, **18**, 89 (1937).

Kluge, T., C. Rezende, D. Wood, and G. Belfort, ''Protein Transmission during Dean Vortex Microfiltration of Yeast Suspensions,'' *Biotech. & Bioeng.*, **65**, 649 (1999a).

Kluge, T., A. Kalra, and G. Belfort, ''Viscosity Effects on Dean Vortex Membrane Microfiltration,'' *AIChE J.*, **45**, 1913 (1999b).

Kroner, K. H., and V. Nissinen, ''Dynamic Filtration of Microbial Suspensions Using an Axially Rotating Filter,'' *J. Memb. Sci.*, **36**, 85 (1985).

Kroner, K. H., V. Nissinen, and H. Ziegler, ''Improved Filtration of Microbial Suspensions,'' *Bio/Tech.*, **5**, 921 (1987).

Kuethe, D. O., and J-H. Gao, ''NMR Signal Loss from Turbulence: Models of Time Dependence Compared with Data,'' *Phys. Rev. E*, **51**, 3252 (1985).

Ligrani, P. M., J. E. Longest, M. R. Kendall, and W. A. Fields, ''Splitting, Merging and Spanwise Wavenumber Selection of Dean Vortex Pairs,'' *Expts. in Fluids*, **18**, 41 (1994).
Liu, S., and J. Masliyah, ''Axially Invariant Laminar Flow in Helical Pipes with a Finite Pich,'' *J. Fluid Mech.*, **251**, 315 (1993).
Luque, S., H. Mallubhotla, G. Gehlert, R. Kuriyel, S. Dzengeleski, S. Pearl, and G. Belfort, ''A New Coiled Hollow-Fiber Module Design for Enhanced Microfiltration Performance in Biotechnology,'' *Biotech. & Bioeng.*, **65**, 3 (1999).
Mallubhotla, H., and G. Belfort, ''Flux Enhancement During Dean Vortex Microfiltration. 8. Further Diagnostics,'' *J. Memb. Sci.*, **125**, 75 (1997).
Mallubhotla, H., E. Nunes, and G. Belfort, ''Microfiltration of Yeast Suspensions with Self-Cleaning Spiral Vortices: Possibilities for a New Membrane Module Design,'' *Biotech. & Bioeng.*, **48**, 375 (1995).
Mallubhotla, H., S. Hoffmann, M. Schmidt, J. Vente, and G. Belfort, ''Flux Enhancement during Dean Vortex Tubular Membrane Nanofiltration. 10. Design, Construction and System Characterization,'' *J. Memb. Sci.*, **141**, 183 (1998).
Mallubhotla, H., M. Schmidt, K-Y. Lee, and G. Belfort, ''Flux Enhancement during Dean Vortex Tubular Membrane Nanofiltration. 13. Effects of Concentration and Solute Type,''**153**, 259 (1999).
Matsson, O. J. E., and P. H. Alfredsson, ''Experiments on Instabilities in Curved Channel Flow,'' *Phys. Fluids A*, **4**, 1666 (1992).
Mees, P. A. J., K. Nandakumar, and J. H. Masliyah, ''Instability and Transitions of Flow in a Curved Square Duct: the Development of Two Pairs of Dean Vortices,'' *J. Fluid Mech.*, **314**, 227 (1996a).
Mees, P. A. J., K. Nandakumar, and J. H. Masliyah, ''Secondary Instability of Flow in a Curved Duct of Square Cross-Section,'' *J. Fluid Mech.*, **323**, 387 (1996b).
Mori, Y., and W. Nakayama, ''Study on Forced Convective Heat Transfer in Curved Pipes,'' *Int. J. Heat & Mass Trans.*, **8**, 67 (1965).
Moulin, P., P. Manno, J. C. Rouch, C. Serra, M. J. Clifton, and P. Aptel, ''Flux Improvement by Dean Vortices: Ultrafiltration of Colloidal Suspensions and Macromolecular Solutions,'' *J. Memb. Sci.*, **156**, 109 (1999).
Nandakumar, K., and J. H. Masliyah, ''Bifurcation in Steady Laminar Flow through Curved Tubes,'' *J. Fluid Mech.*, **119**, 475 (1982).
Narasimha, R., and K. R. Sreenivasan, ''Relaminarization of Fluid Flows,'' *Advances Applied Mechanics*, C-S. Yih, ed., Vol. 19, Academic Press, New York, p. 221 (1979).
Pangrle, B. J., E. G. Walsh, S. C. Moore, and D. DiBiasio, ''Magnetic Resonance Imaging of Laminar Flow in Porous Tube and Shell Systems,'' *Chem. Eng. Sci.*, **47**, 517 (1992).
Sreenivasan, K. R., and P. J. Strykowski, ''Stabilization Effects in Flow through Helically Coiled Pipes,'' *Exp. in Fluids*, **1**, 31 (1983).
Vera-Colon, M., ''Nuclear Magnetic Resonance Studies of Flowing Liquids,'' PhD Thesis, Purdue University, West Lafayette, IN (1986).
Yanase, S., N. Goto, and K. Yamamoto, ''Dual Solutions of the Flow through a Curved Tube,'' *Fluid Dynamics Res.*, **5**, 191 (1989).
Yao, S., ''Nuclear Magnetic Resonance Flow Micro-imaging,'' PhD Thesis, University of New South Wales, Australia (1995).

Manuscript received Dec. 6, 1999, and revision received Aug. 24, 2000.